LANGMUIR Article
Cite This: Langmuir 2018, 34, 5444−5453
pubs.acs.org/Langmuir

Influence of Substrate Bonding and Surface Morphology on Dynamic Organic Layer Growth: Perylenetetracarboxylic Dianhydride on Au(111)

Thomas Schmidt,*[,†,‡] Helder Marchetto,[‡] Ullrich Groh,[†] Rainer H. Fink,[§] Hans-Joachim Freund,[‡] and Eberhard Umbach[†,‡]

[†]Experimentelle Physik, Universität Würzburg, Am Hubland, 97074 Würzburg, Germany
[‡]Chemische Physik, Fritz-Haber-Institut der Max-Planck-Gesellschaft, Faradayweg 4-6, 14195 Berlin, Germany
[§]Physikalische Chemie 2, Friedrich-Alexander-Universität Erlangen-Nürnberg, Egerlandstr. 3, 91058 Erlangen, Germany

Supporting Information

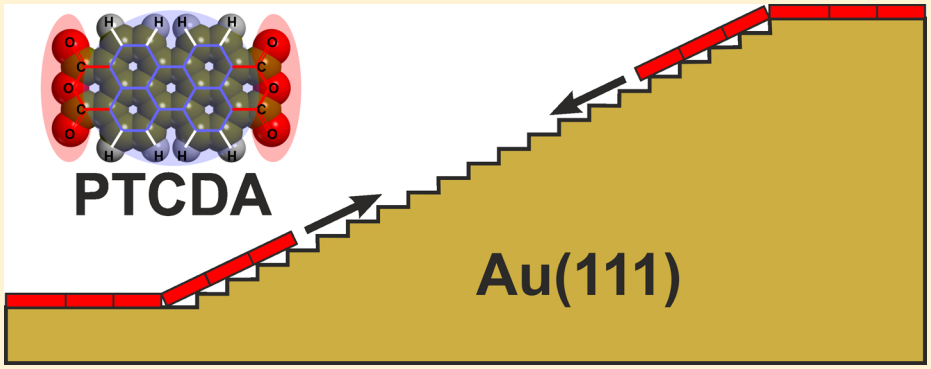

ABSTRACT: We investigated the dynamics of the initial growth of the first epitaxial layers of perylenetetracarboxylic dianhydride (PTCDA) on the Au(111) surface with high lateral resolution using the aberration-corrected spectro-microscope SMART. With this instrument, we could simultaneously study the different adsorption behaviors and layer growth on various surface areas consisting of either a distribution of flat (111) terraces, separated by single atomic steps ("ideal surface"), or on areas with a high density of step bunches and defects ("realistic surface"). The combined use of photoemission electron microscopy, low-energy electron microscopy, and μ-spot X-ray absorption provided a wealth of new information, showing that the growth of the archetype molecule PTCDA not only has similarities but also has significant differences when comparing Au(111) and Ag(111) substrate surfaces. For instance, under otherwise identical preparation conditions, we observed different growth mechanisms on different surface regions, depending on the density of step bunches. In addition, we studied the spatially resolved desorption behavior which also depends on the substrate morphology.

1. INTRODUCTION

The interfaces of organic thin films and metals are of prime scientific interest for applications as well as for the fundamental understanding of heterointerfaces in general. Examples of applications are organic photovoltaics,[1,2] organic field-effect transistors,[3] and organic light-emitting displays.[4,5] Their properties often strongly depend not only on the molecules but also on the interfaces between the organic material and metallic contact and on the growth behavior of the organic thin film on a substrate. Although it is well-established that the relative positions of the electronic levels responsible for charge injection are related to the electronic potentials and chemical interaction between the organic material and metal,[6,7] it is less well-known that the interface and geometric structure of the organic layer may drastically influence the optical properties such as quenching and fluorescence yield.[8−10] Thus, for the optimization of the properties of organic devices, it is of decisive importance to fundamentally understand the interplay between preparation and function, and especially between interface, thin-film growth as well as geometric and electronic structures.

Recently, we have published several papers which address the interplay between substrate morphology, preparation parameters, formation of the interface, and further growth of organic layers.[11−17] In these papers, we have concentrated on the system perylenetetracarboxylic dianhydride (PTCDA) on Ag(111) and its vicinal surfaces. We have discovered large-scale reconstructions,[15−17] the formation of regular mesoscopic patterns,[15] the occurrence of a wealth of molecular superstructures,[17] different nucleation processes,[12,13] the develop-

Received: February 12, 2018
Revised: April 12, 2018
Published: April 26, 2018

DOI: 10.1021/acs.langmuir.8b00493
Langmuir 2018, 34, 5444−5453

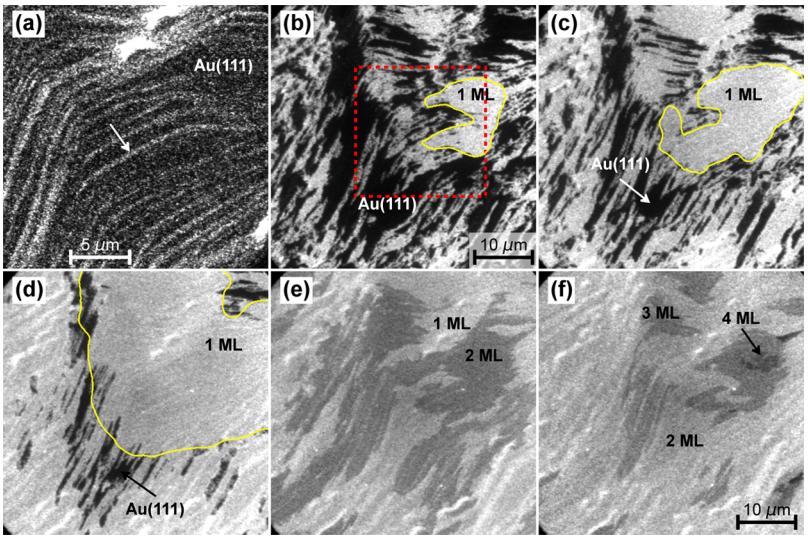

Figure 1. UV-PEEM images of the growth of PTCDA/Au(111) at 470 K. The deposition rate is 0.22 ML/min. Nominal PTCDA coverages in the sequence (a–f) are 0, 0.5, 0.7, 0.9, 1.5, and 2.5 MLs. The acquisition times are 4 s every 6 s; image (a) is the average of a stack of 10 images to enhance the visibility of low intensity features of the substrate-like step bunches (see arrow). The latter appears as bright lines across the otherwise dark (i.e., clean) substrate. Image (a) has a twofold higher magnification with respect to the rest of the sequence; the imaged region is highlighted by a square in (b). The scale bar in (e) is 5 μm. In (b–d), two different types of film phases exist simultaneously: one is highly defective (i.e., rich of holes with sharp edges) and one is a fully closed, homogeneous monolayer (indicated by a surrounding yellow line). The latter rapidly expands as a function of coverage as seen in (c,d). In (e,f), areas of higher coverages are indicated.

ment and behavior of rotational and mirror domains for the first two layers,[14,18] and the dependence of various growth mechanisms on preparation parameters and substrate morphology.[12,13] Nearly, all of these observations were strongly correlated with the chemisorptive bonding between PTCDA and the Ag substrate. Therefore, it is an obvious next step to investigate the differences that occur when a significantly weaker bonding occurs under otherwise very similar conditions. Thus, we have chosen the Au(111) surface as a substrate in the present work to study the differences in the dynamic behavior of organic film growth using the same prototype molecule PTCDA. It turns out that both growth mechanisms, Stranski–Krastanov as well as Frank–van der Merwe, also occur on Au(111), but that their occurrence depends not only on the temperature but also strongly on the surface morphology.

The adsorption and growth of PTCDA have been studied much less on Au(111) than on Ag(111). Nevertheless, essential findings have been documented and discussed. The monolayer of PTCDA is formed in the usual herringbone structure on top of the $(22 \times \sqrt{3})$ reconstructed Au(111) surface where the reconstruction remains essentially unaffected which has been investigated by scanning tunneling microscopy (STM),[19−22] low-energy electron diffraction (LEED),[20] and spot-profile analysis LEED (SPA-LEED).[23] It has even been found[23] that both a "distorted carpet", with a true point-on-line relation between the adsorbate and substrate, and a "rigid carpet", with only average point-on-line relation, can occur depending on preparation conditions. This finding indicates only weak bonding of PTCDA on Au(111) in contrast to Ag(111)[24] which has directly and indirectly been derived by ultraviolet photoelectron spectroscopy (UPS),[21] scanning tunneling spectroscopy (STS),[21,22] and normal-incidence X-ray standing wave (NIXSW)[25] investigations, which yielded only minor peak shifts (UPS and STS) and a significantly larger vertical bonding distance relative to the substrate comparing Au(111) and Ag(111) (NIXSW: 3.27 vs 2.86 Å[25]). This difference in the bonding mechanism and strength has been confirmed by detailed density functional theory calculations comparing the bonding of PTCDA on the (111) faces of Cu, Ag, and Au.[26] Very little has been published on the growth behavior of PTCDA thin films on Au(111),[27−29] and those published studies use integral techniques (X-ray diffraction and soft X-ray reflectivity) which cannot provide direct insight into morphological and structural details. The present study presents new data with respect to the initial stages of (epitaxial) layer growth and their dependence on surface morphology and preparation parameters.

2. EXPERIMENTAL SECTION

The instrument used for the present experiments is the SMART spectro-microscope[30−32] installed at the UE49-PGM beamline of the BESSY-II storage ring of the Helmholtz-Center Berlin for Material and Energy (HZB). SMART is equipped with an aberration corrector, compensating simultaneously both chromatic and spherical aberrations,[33−35] and with an imaging energy filter. A lateral resolution of better than 2.6 nm was experimentally demonstrated in the low-energy electron microscopy (LEEM) mode.[36,37] The design of the specimen chamber enables the in-situ deposition of, for example, organic material under grazing incidence (20°) onto the sample surface at the measurement position in front of the objective lens. The sample temperature is regulated by radiative and electron-bombardment heating and monitored by a thermocouple. Thus, the growth or desorption of the PTCDA film could be directly observed in real time. For deposition, a Knudsen cell-type evaporator was used. The deposition rate was maintained constant to about 0.08 ML/min (ML = monolayer coverage) by stabilizing the evaporator temperature at 650 K. One monolayer coverage corresponds to the deposited amount required to saturate the first PTCDA layer (of parallel oriented molecules) on the surface at 330 K. At this temperature, desorption can be neglected. The base pressure of the measurement chamber was $<3 \times 10^{-10}$ mbar. A potential influence of the instrumental setup on the growth has been carefully checked and could be excluded.[12] The kinetic energy of the electrons at the sample surface in the LEEM experiments was reduced below 5 eV which is

DOI: 10.1021/acs.langmuir.8b00493
Langmuir 2018, 34, 5444−5453

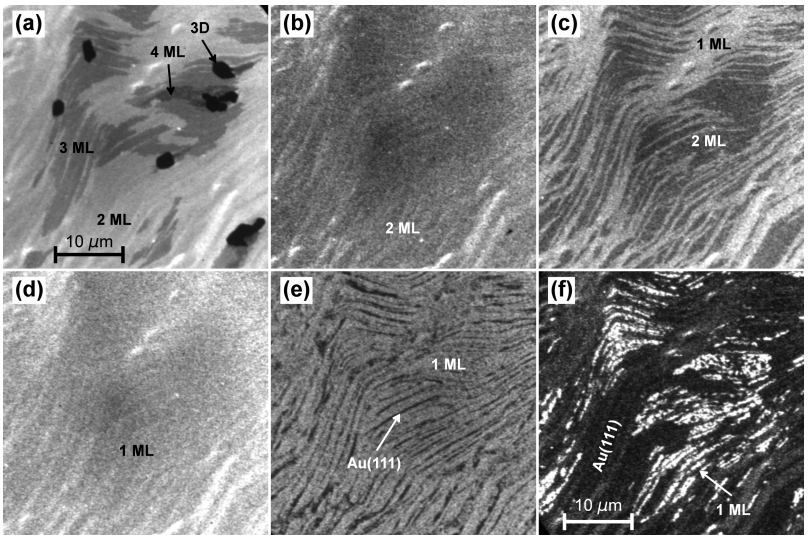

Figure 2. UV-PEEM image sequence of the desorption of 6.6 ML of PTCDA from the Au(111) surface. The temperature was increased from 470 to 690 K at a rate of 7.3 K/min. The calculated coverages are 6.6, 2, 1.35, 1, 0.8, and 0.15 ML for (a–f), respectively. The sequence has been taken from the same surface region as in Figure 1. The magnification is the same in all images; the scale bar in (e) is 5 μm. Areas of uncovered Au(111), 1 ML, 2 ML, and more ML PTCDA coverage as well as 3D islands are indicated in the images.

about the threshold below which no beam-induced damage is observed.

A Au(111) single crystal oriented within an accuracy better than 0.2° has been cleaned by repeated cycles of Ar sputtering (600 eV, 1 μA, 5 × 10^{-5} mbar, 15 min, room temperature) with subsequent annealing at 700–800 K for about 15 min. The cleaning progress was checked by photoemission electron microscopy (PEEM), LEEM, LEED, and X-ray photoelectron spectroscopy.

In the UV-PEEM mode, ultraviolet light from a Hg discharge lamp (maximum intensity at $h\nu$ = 4.9 eV) releases electrons from the surface by photoemission. The emitted electrons are directly imaged on a two-dimensional (2D) detector and recorded over time by a charge-coupled device camera. The contrast mechanism is determined by the work function of the surface and by attenuation of the electrons emitted from the Au substrate by deposited PTCDA molecules. In the near-edge X-ray absorption fine structure (NEXAFS)-PEEM mode, monochromatized X-rays from the UE49-PGM undulator beamline at BESSY are used to directly image the emitted secondary electrons on the 2D detector in real time. In this case, the X-ray polarization could be switched between s-polarization (with *E*-vector parallel to the surface) and p-polarization (with an *E*-vector component almost perpendicular to the surface) by shifting the magnetic poles of the undulator.[38] In the LEEM mode, electrons from an electron gun are decelerated near the surface, back-diffracted by the outermost surface layers, and recorded as a spatially resolved image. The contrast mechanism in this case is governed by the local surface reflectivity and by interference effects that occur upon electron reflection at different surface layers.[39]

3. RESULTS AND INTERPRETATION

3.1. Nucleation and Growth of the First Layers. Figure 1 shows the initial stages of PTCDA layer growth on a clean Au(111) surface at 470 K. Figure 1a presents a UV-PEEM image of the initial, that is, pure surface, prior to PTCDA deposition. The displayed sample area was chosen as statistically representative exhibiting a number of characteristic "patterns" of surface structures: black areas represent (111) terraces that are separated from each other by single atomic steps, discernible here as fuzzy bright lines. The clean and (22 × $\sqrt{3}$) reconstructed Au(111) terraces appear black because the work function of this surface is ~5.3 eV and hence higher than the photon energy of the UV lamp (4.9 eV), thus suppressing photoemission from these terraces. Steps or adsorbed molecules reduce the local work function and hence enable photoemission from the substrate; they are then seen as bright lines or areas because of their higher electron emission rate. The fact that PTCDA molecules adsorbed in the monolayer regime on Au lower the work function is due to their weak (physisorptive) bonding to the substrate.[40] Such a lowering is commonly found for physisorbed molecules on high work function surfaces and is understood as a kind of Pauli repulsion effect.[41,42] This is in contrast to PTCDA adsorption on Ag(111) for which chemisorptive (i.e., covalent) bonding has been proven by strong changes in the UPS, NEXAFS, or high-resolution electron energy loss spectra,[24,43–47] which shows a work function increase by more than 0.2 eV.[13,14] Such spectroscopic changes are not observed for PTCDA on Au[24] (see also below).

Figure 1b displays the same area of the surface (on a twofold larger scale) covered by about half a monolayer of PTCDA. The molecules nucleate on the (111) terraces, and the nuclei grow in size as coverage increases. On some areas of the surface, the nuclei merge and form large compact islands without holes. Because of this coalescence, they seem to rapidly increase in size, faster than the smaller islands around the nuclei. One example of such a fast growing island is indicated by the yellow boundary lines in Figure 1b–d (see also movie in the Supporting Information). This special type of growth process, which only occurs in the monolayer regime, has not been observed before. The sequence of images of Figure 1b–d which represent the growth behavior of the monolayer regime, also shows that the areas between steps or step bunches are filled separately. Thus, the layer has numerous empty spaces (holes) which are only slowly filled and are finally closed when the monolayer is completed. Note that all of this happens before the second layer starts growing.

Figure 1e,f displays snapshots of the growth of further layers. The dark areas of Figure 1e represent the second layer that covers about half of the surface after deposition of 1.5 ML PTCDA. The second layer is darker in PEEM because photoemission from the substrate is further attenuated by this

DOI: 10.1021/acs.langmuir.8b00493
Langmuir 2018, 34, 5444–5453

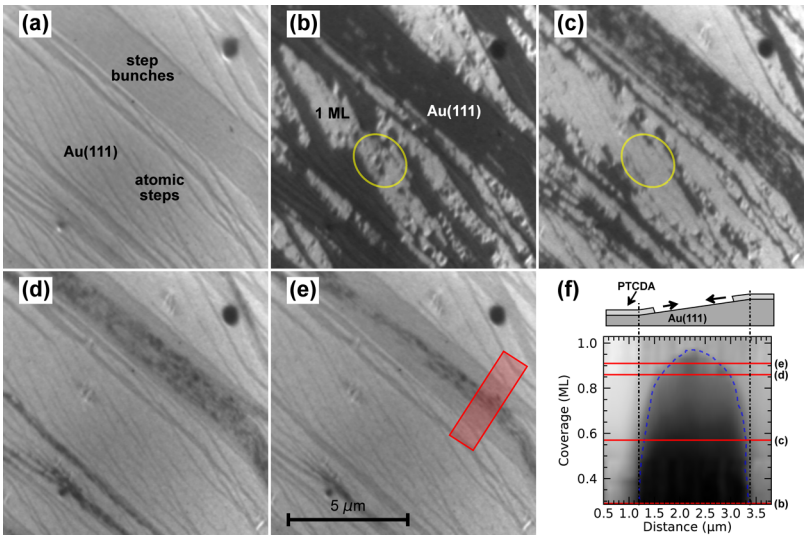

Figure 3. (a–e) LEEM images recorded with 3 eV electron energy representing the growth of 1 ML of PTCDA on a selected Au(111) surface region at 380 K. In (a), surface areas with different substrate morphologies are indicated. The coverages are 0, 0.29, 0.57, 0.86, and 0.91 for (a–e), respectively; the brighter regions are PTCDA covered. The magnification is the same in all images; the scale bar in (e) is 5 μm. In (b,c), the same substrate region is highlighted by a yellow ellipse to show the development of the monolayer film as a function of coverage. In figure (f), the coverage evolution during growth on a substrate area with a high density of step bunches during growth is displayed. The line profiles of figure (f) were taken at increasing coverage along the long side of the red rectangle highlighted in (e) while averaging along the perpendicular direction. The horizontal red lines indicate the line profiles of figures (b–e). The sketch at the top of figure (f) pictures how PTCDA grows from flat regions into the highly stepped region.

additional layer. Apparently, nucleation of the second layer takes place preferably on smooth areas of the substrate (e.g., indicated by "2 ML"), whereas areas with many step bunches and defects (e.g., indicated by "1 ML") are only covered by the second layer near its completion. It is noted that also the second layer is completely filled before significant amounts of the third layer nucleate. This and further layers then grow simultaneously, that is, islands are formed on top of the second layer which grow simultaneously in height and size, as seen after deposition of 2.5 ML in Figure 1f and of 6.6 ML in Figure 2a, and as seen in the complete growth movie (see the Supporting Information).

This behavior is typical for a kind of Stranski–Krastanov growth mode, which often occurs if the adsorption of the first layer(s) to the substrate is strong enough to result in a well-ordered film commensurate to the substrate but strained as compared to the bulk structure, for example, a layer of a molecular crystal. Then, for higher layers, the molecular film relaxes forming crystallites in one of the known crystalline structures, here α- or β-PTCDA.[48,49] The interesting question whether the first two layers remain strained (and hence in registry with the substrate) upon the formation of three-dimensional (3D) islands on top (similar to that for PTCDA on Ag(111)) or whether they also relax when a thicker film is formed could not be answered here.

Two further observations are worth mentioning: first, the deposited molecules diffuse over very large distances (several tens of micrometers) on the Au(111) substrate as well as on the first PTCDA layers, and they diffuse easily across single surface steps before they get trapped at nucleation centers or fill the holes within the first layer(s). Long diffusion lengths at these temperatures have also been observed for the growth of PTCDA on other metal surfaces.[12−14] A possible explanation for this behavior is that the molecules—in addition to their kinetic energy and in contrast to the substrate atoms—possess a considerable amount of internal thermal energy (excited internal vibrational and bending modes) when they leave the ∼650 K hot Knudsen cell, and that these internal degrees of freedom are not immediately accommodated by the substrate when the molecules arrive at and diffuse over its surface. Second, the molecules prefer smooth substrate areas without step bunches to nucleate and to form large 2D islands which are elongated parallel to steps or step bunches. This information may be deduced from the development of the layers shown in Figure 1 which occurred preferably on areas with few single atomic steps. We assume that the reason for this contra-intuitive behavior is that the transfer of the internal energy preferably occurs to neighboring "cold" (i.e., already adsorbed and accommodated) molecules which have similar internal modes to which those of the hot molecules can resonantly couple. Thus, they do not couple to inhomogeneities of the substrate such as steps, which are available to accommodate the energy of a diffusing molecule because the interaction with the Au substrate is weak. This leads to the following question: is thermal desorption reversible with respect to adsorption?

3.2. Desorption—Reversed Growth? Figure 2 displays some representative snapshots from a desorption series, also recorded as a movie (see the Supporting Information), taken at the identical surface area displayed in Figure 1. Figure 2a (nominal coverage 6.6 ML) shows the situation at 470 K directly after stopping the PTCDA deposition: some dark areas are seen on top of a gray background which is representative for a molecular double layer. The dark areas stem from three or four layers or even represent 3D islands as indicated in the figure. As observed for PTCDA/Ag(111),[12] the metastable fourth layer shrinks in size and is "eaten up" by the 3D islands as soon as the PTCDA flux is turned off. Upon heating to 500 K, the third layer and the 3D islands disappear first and a homogeneous double layer remains (Figure 2b). Further heating to 520 K desorbs more than half of the second layer (Figure 2c; coverage 1.35 ML). The remaining part desorbs upon heating to 575 K (Figure 2d). Heating to 650 K desorbs

DOI: 10.1021/acs.langmuir.8b00493
Langmuir 2018, 34, 5444−5453

20% of the monolayer (Figure 2e) and heating to 660 K further 65% (Figure 2f). Finally, all PTCDA molecules are removed at 680 K (not shown).

Three observations are important: first, PTCDA on Au(111) may be completely removed by heating in contrast to PTCDA on Ag(111) where the monolayer remains on the surface and decomposes upon heating to more than about 720 K.[50] Second, the second and especially the first layer are more strongly bound than additional layers, which indicates the influence of the substrate even for physisorption. Third, the desorption process of the second and first layers occurs equally likely from different regions of the surface, that is, desorption does not occur from, for example, the rim of large islands. However, the situation is different on the microscopic scale: in both cases, desorption starts at steps or step bunches (bright lines in Figure 2c and dark lines in Figure 2e), and the molecules on flat surface areas between the steps desorb last (Figure 2f). The growth of the first PTCDA layer starts on the terrace; therefore, Figures 2f and 1b show a corresponding situation, which is different in detail. However, the closure of the first layer (Figure 1d) is clearly different from the comparable coverage during desorption in Figure 2e. The first layer islands not only grow along but also grow across steps and close at step bunches last, and the growing islands are very large. The desorption behavior, however, is clearly different from the adsorption behavior because desorption starts at many more points that were closed at the end of the first layer adsorption. Thus, at each coverage, there are many more (small) shrinking islands upon desorption than growing (large) islands upon adsorption. The reason for this difference is probably the mechanism of island growth upon adsorption which is most likely due to the accommodation process of the "hot" deposited and diffusing molecules at the rim of islands. Even though both processes were not performed under identical conditions (adsorption at 470 K, desorption of the ML at 650−680 K), we must conclude that there is no microscopic reversibility because of the accommodation process in the adsorption case.

3.3. Influence of Surface Morphology on the Development of the First Layers. Next, we study the influence of the surface morphology in more detail using the LEEM mode. The contrast mechanism in this mode is based on reflectivity and interference effects, as discussed above. On contrary to the PEEM mode, attenuation does not play a role for the contrast mechanism, but interference effects emphasize details of the surface morphology such as single atomic steps. Thus, by using the LEEM mode, surface morphologies can be investigated in great detail. For instance, in Figure 3a, the selected surface region has been conveniently chosen to include in a single field of view (FoV) the main surface structures found otherwise distributed on the surface: large terrace areas with single atomic steps and areas with high step densities (step bunches). Thanks to the high lateral resolution in the LEEM mode (2.6 nm[36]) and the contrast mechanism one may easily identify single atomic steps.

Here, we study the development of the first layer with increasing coverage (Figure 3b−e). Again, these (representative) figures are selected from a large data set. It is clearly seen that nucleation and growth of first layer islands preferentially occur on surface areas with monoatomic steps and large smooth areas in between. Although few and small islands are also seen in the step-bunch regions, these areas remain rarely covered until the smooth areas are completely filled. Only then, the step-bunch areas are successively filled by PTCDA islands starting from the edges of the step-bunch areas and growing toward their center (see Figure 3d,e).

The latter observation has been evaluated in more detail for the red area indicated in Figure 3e; the result is displayed in Figure 3f where line profiles along the long side of the red rectangle are plotted versus coverage. For noise reduction, the line profiles were generated by averaging along the short side of the red rectangle. As described for the previous LEEM images, the brighter regions are covered by one monolayer of PTCDA and the darker represents the bare substrate. The blue dashed line serves as a guide for the eyes to follow the evolution of the growth of the PTCDA layer as a function of overall coverage. The shape of this curve indicates that the smooth areas outside the step bunches are covered first, and only after those are nearly filled (Figure 3c, 0.57 ML) the covered area propagates from the rims toward the center of the step-bunch region. The velocity of this growth front increases at 0.86 ML (Figure 3d), when all other areas are completely closed and thus all incoming PTCDA molecules are now incorporated on the stepped surface area.

One more observation is worth mentioning: for low coverages, the PTCDA islands are rather inhomogeneous and defective as seen, for example, within the yellow ellipse of Figure 3b. The layer has many holes and inhomogeneities, indicating incomplete filling of the first layer and perhaps even different orientations (e.g., inclined molecules) or geometric structures (e.g., different superstructures or rotational domains). If the coverage increases, a kind of phase transition occurs. Starting from different nucleation centers, "wave fronts" move across the surface filling the holes, rendering the adsorbate layer much more homogeneous (see yellow ellipse in Figure 3c). This observation is compatible with the high-speed expansion of the yellow island in Figure 1 that occurred under similar but not identical conditions and was observed on a larger scale in the PEEM mode. We explain this coverage-induced, long-range rearrangement of the adsorbate layer by a lateral and structural optimization process of the entire adsorbate layer. The integration of additional molecules in an ordered, densely packed fashion leads to a gain in total energy, although the entire layer has to be rearranged. The observation that such effects can occur over distances of several microns (see Figure 1) is probably due to the fact that the molecules are weakly bonded to the substrate and the vertical bonding potential is only weakly corrugated as compared to more strongly bound systems.

More insight may be obtained by a quantitative evaluation using an Arrhenius plot of the island density as a function of the temperature in the monolayer regime in order to derive an apparent activation energy for diffusion (Figure 4). Here, we compare the numbers derived from PEEM and LEEM data, and note that they result in different activation energies. We think that not only the considerably higher spatial resolution of the LEEM data leads to the detection of more islands and hence to higher densities but also experimental differences such as different temperature calibrations and different surface morphologies that could have had a significant influence because the UV-PEEM and LEEM experiments were performed at different times with different sample holders, and so forth. Thus, we arrive at different values for the activation energy as indicated in the figure. The two dotted lines yielding two different numbers hence provide a possible range of values (corresponding to an error bar), with the higher value (0.3 eV) obtained by including the LEEM data and the

DOI: 10.1021/acs.langmuir.8b00493
Langmuir 2018, 34, 5444−5453

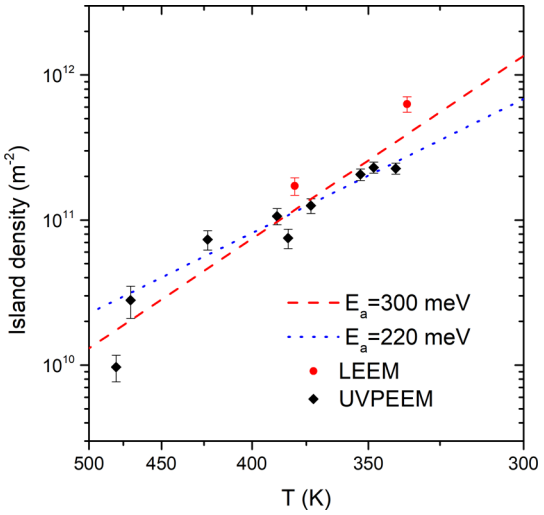

Figure 4. Arrhenius plot of the nucleation density of the PTCDA monolayer on Au(111) as a function of substrate temperature for two imaging methods. Two lines, dashed and dotted, are fitted to the data in different ways (as described in the text); they result in two different activation energies (300 and 220 meV) which indicate the range of possible activation energies.

high-temperature UV-PEEM data point, whereas omitting them, a value of 0.22 eV is obtained. A detailed discussion of the implications of the activation energies on the molecular diffusion will follow in Section 4.

3.4. Influence of Surface Morphology on the Growth Mode of Thin Films. It has often been observed that the growth behavior strongly depends on the substrate temperature, which is not surprising. However, the observation that for a particular system (PTCDA/Ag(111)) between about 200 and 450 K, all three different growth modes (Volmer–Weber, Frank–van der Merwe, and Stranski–Krastanov) can be found is interesting.[12] This means that for all practical purposes, the adsorption temperature has a major influence on the molecular structure and hence on the electrical and even optical properties, in agreement with previous findings.[10]

In the present study, we present another surprising observation, namely, that two growth modes occur simultaneously on the same surface under identical conditions (temperature and molecular flux) depending only on the particular surface morphology. This is displayed in Figure 5, which shows LEEM results obtained during PTCDA deposition at 350 K. On the bare surface (Figure 5a), one observes again areas with a high density of step bunches as well as areas with only atomic steps and large smooth terraces in between (as indicated in Figure 5a). Upon deposition of PTCDA, one can follow a typical layer-by-layer (Frank–van der Merwe) growth for several layers in the areas with only atomic steps, whereas on the step bunches, 3D objects (PTCDA crystallites) appear after completion of the second layer. This development is best seen in the movie which is provided in the Supporting Information, thereby proving that the microscopic observation of the dynamic development of an adsorbate layer may be very helpful for extracting additional information compared to static measurements.

3.5. Molecular Orientation and Bonding. Seeing the 3D islands or the inhomogeneity within the first layers, one may ask the question whether the molecules all exhibit the same orientation or whether crystallites with different structures (and hence inclined molecular angles) exist on the surface. The answer can be derived from Figure 6a which displays spatially

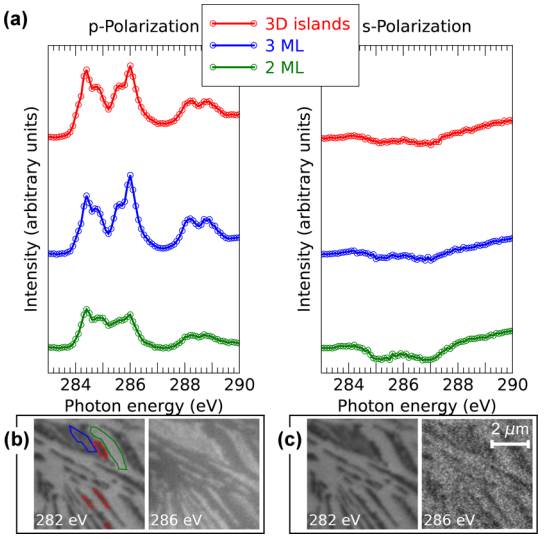

Figure 6. (a) NEXAFS spectra of PTCDA on Au(111) for different PTCDA coverages (see color code in the inset) for p-polarization (left) and s-polarization (right). The polarization vectors for p- and s-polarization are 20° and 90° with respect to the normal of the sample surface, respectively. (b,c) Two NEXAFS-PEEM images recorded with photon energies below the adsorption edge (282 eV) and in the absorption maximum (286 eV) using p- and s-polarized lights. The colored curves in (a) have been obtained by integrating over the colored regions shown in (b)-left. The magnification is the same in all images; their field of view is 7.2 × 7.2 μm^2.

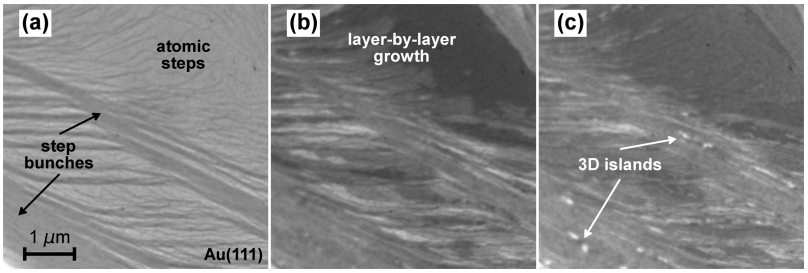

Figure 5. LEEM images recorded with 3 eV electron energy representing the multilayer growth of PTCDA on the same Au(111) surface region at 350 K. The coverages in the sequence (a–c) are 0, 3.8, and 6.8 ML, respectively. The imaging conditions were chosen such that thicker layers have different gray tones (see, e.g., in (b)), whereas 3D islands appear white in (c). The different growth regimes are indicated in the figure. The magnification is the same in all images; the scale bar in (a) is 1 μm.

DOI: 10.1021/acs.langmuir.8b00493
Langmuir 2018, 34, 5444–5453

resolved NEXAFS spectra for two different polarization directions of the incoming X-rays and three different areas on the surface. The latter is color-coded such as the spectra and is indicated in the NEXAFS-PEEM maps below (Figure 6b left), taken at two different absorption energies. These two energies were chosen either below the absorption edge (282 eV) or in the peak of maximum absorption (286 eV), leading to a reversal of the contrast in the maps shown in Figure 6b. For the map recorded below the absorption edge, the detected electron emission stems mainly from the substrate and is attenuated by the molecular layer (which hence appears dark), whereas in the case for maximum absorption, the emission mainly stems from the molecules (which hence appear bright). For the spectra and maps taken with s-polarization (Figure 6c), there is obviously no absorption maximum and hence also no contrast reversal in the maps.

In Figure 6a, we have concentrated on the energy range in which the π-resonances occur. From the data of Figure 6a, one may derive two important pieces of information: first, the strong dichroism for p- and s-polarization clearly indicates that the molecules are oriented parallel to the substrate surface using the common selection rules.[51] It is of course interesting that this is apparently the case for the double and triple layers (and hence for the first layer) as well as for the 3D islands. This result is unambiguous although the spectra exhibit different noise levels, which is due to the very small areas recorded, and show small differences (especially for s-polarization), which are due to the known normalization difficulties at the carbon edge.[52] The second observation is that all spectra are very similar to each other and to those of thick PTCDA films (or gas-phase PTCDA) but are very different from those of the PTCDA monolayer on Ag. This is another indication that the bonding of PTCDA to Au is weak and can be described as physisorption, whereas on the Ag surface, the molecules are chemisorbed changing the electronic molecular structure significantly.[24,44−47]

4. DISCUSSION—COMPARISON WITH AG(111)

Summarizing the presented data, we conclude that PTCDA adsorption on Au(111) is in some respect similar to that on Ag(111) but that there are also significant differences. Those are most likely connected with the different interface bondings in both cases as discussed above but may also arise from differences in the surface morphology. We note that the significantly stronger bond to Ag(111) may lead to a complete, large-scale reorganization of the surface involving PTCDA-induced step bunching such that vicinal faces are created by large mass transport of Ag atoms induced by the adsorbate bonding.[15−17] In contrast, the Au(111) surface is hardly affected by PTCDA adsorption. This is underlined by the observation that the well-known $(22 \times \sqrt{3})$ reconstruction of the clean Au(111) surface remains unchanged upon PTCDA adsorption,[23] thus indicating the weakness of the adsorption bond. This is further corroborated by the electronic data of the monolayer which are very similar to those of thick PTCDA films (see above and refs 24, 44, 46).

Therefore, it seems surprising that only few differences are observed between the growth behavior of PTCDA on those two substrates. Perhaps most surprising is the difference in activation energies for diffusion in the first layer. On Ag(111), two different regimes with different activation energies of diffusion were distinguished:[13] the value on smooth surface areas is 130 meV, whereas on rough areas (high step density), the derived value ("10 meV") is temperature-independent because the island formation is determined by the substrate defects and not by the diffusion length. The values derived from the Arrhenius plots for PTCDA on Au(111) lie between 220 and 300 meV (see above and Figure 6) and hence are significantly larger than those derived for PTCDA on Ag(111). At first glance, this appears surprising because the chemical bonding of the monolayer to the substrate is much stronger for Ag(111) than for Au(111), indicating that bonding energy and activation energy for diffusion have little to do with each other.

What is the reason for the higher activation energy for PTCDA on Au(111), or better, the relatively low activation energy for PTCDA on Ag(111)? We suggest that the activation energy of diffusion on Au(111) represents the regular case, that is, that bonding sites, steps, and step bunches of the substrate are the natural obstacles which determine the diffusion behavior. This is in agreement with the observation that there are differences for the diffusion over terraces and across single atomic steps as compared to diffusion across step bunches because we could observe a delayed filling of the monolayer on step bunches (see, e.g., Chapter 3.3 and Figure 3d−f), whereas we did not find quantitative differences for the activation energies between different areas on the surface (as on Ag(111)).

Why is the activation energy for diffusion on Ag(111) different and why is it so low? We suggest that this is due to a kinetic precursor state, which has been found in many adsorption studies in the past (see, e.g., ref 53). Such precursor states occur if the deposited hot atoms or molecules remain in a diffusive, weakly bound state until they find a suited adsorption site where they finally stick, possibly after having overcome an activation barrier. For PTCDA on Ag(111), this activation barrier may arise from the fact that the molecule is being distorted with respect to its original molecular structure[54] when it is finally chemisorbed either forming an ordered overlayer (at RT or higher temperatures) or a kind of chemical precursor state[55] which is very different from the kinetic precursor because it is also chemisorbed and occurs at low temperatures (e.g., 150 K) but shows only short-range order. This adsorbate state has a slightly different geometric structure and electronic signature as compared to the stable final adsorption state and is irreversibly transferred into this state upon mild annealing (e.g., at room temperature).

The small activation energy on smooth Ag(111) is then due to the small potential corrugation that the weakly bound kinetic precursor state senses. The negligible activation energies on rough Ag surface areas may then be related to an even smaller interaction (and hence potential corrugation) between the steps and the precursor state. This appears reasonable because a physisorbed large molecule has less nearest neighbors (metal atoms) on an atomically rough surface as compared to a smooth surface.

In addition to the diffusion barriers, we observed a few more differences, which are most likely related to the different bonding to the substrates. For instance, the fact that PTCDA molecules on Au(111) first nucleate on the terraces of bare areas with few (monoatomic) steps and only at the end of the filling of the monolayer cover the step bunches, whereas on Ag(111), they first adsorb at steps or step bunches and then on the (111) terraces is certainly related to the bonding. Also, the observation made in the present work that in the first half of the monolayer growth on Au(111), sometimes islands grow inhomogeneously and exhibit holes that are filled before

DOI: 10.1021/acs.langmuir.8b00493
Langmuir 2018, 34, 5444−5453

completion of the monolayer, is different from the observations made on Ag(111). Especially the rapid, wavelike formation of large islands by integration of smaller islands and by filling additional molecules into the holes and spaces is special in the present case and has not been observed before, for example, for PTCDA on Ag(111).[12] We argued above that this reorganization of the adlayer requires a reorganization (e.g., shifting) of already existing islands and hence a coordinated change of many molecules in the adsorbate layer. This is only possible if the lateral corrugation of the bonding potential of the metal substrate is small compared to the intermolecular interaction. This argument is in agreement with the observation that on Au(111), the herringbone structure of the substrate survives the PTCDA adsorption, whereas on Ag(111), large-scale reconstructions of the substrate atoms are induced by the PTCDA adsorption.[15−17]

As a further difference in the desorption behavior of PTCDA on Au(111), on Ag(111), we found that the first layer is not desorbed but dissociates upon heating. For higher layers, we observed complete reversibility, that is, the movie (Supporting Information) displaying desorption gives the impression as if the adsorption movie was displayed in the reverse direction.[12] On Au(111), adsorption and desorption of the second and higher layers are also essentially reversible (compare Figures 1 and 2, and see Chapter 3.2). However, the monolayer can also thermally be desorbed, and its desorption and adsorption behaviors are not reversible. Adsorption and nucleation on Au(111) first occur on the flat terraces between single atomic steps, and later the stepped areas are being covered before completion of the first layer. Reversibility would imply that desorption from areas that are covered first desorb last, but here the molecules first desorb from the flat terraces (as seen by comparing Figure 1b,d with 2f,e). To our knowledge, such a microscopic irreversibility in adsorption/desorption processes has not yet been observed for large molecular adsorbates.

Finally, we note an additional difference between the two substrate surfaces: on Au(111), we found unexpectedly that two different growth modes occur simultaneously under identical preparation conditions (temperature and molecular flux) only dependent on the surface morphology (see Figure 4 and Chapter 3.4). In surface regions with large flat terraces separated from each other only by single atomic steps, the PTCDA layer grows layer-by-layer in a nearly perfect Frank−van-der-Merwe growth mode. However, in surface regions with a high density of steps and multiatomic steps, that is, step bunches, only the first two layers grow layer-by-layer followed by the growth of 3D crystallites or 3D islands which is usually called the Stranski−Krastanov growth. Also, on Ag(111), we observed both growth modes but they were only temperature- (and most likely also flux-) dependent but independent of the surface morphology.

5. CONCLUSIONS

We emphasize here that an important finding of the present work is this dependence of the growth mechanism on surface morphology because it means that the result of the substrate surface preparation can strongly influence the properties of thin organic films. For instance, if the preparation has resulted in a flat surface with few atomic steps and large (111) areas in between, the PTCDA film growth may lead to a rather homogeneous and ordered film of several well-stacked layers. If, however, the preparation resulted in a microscopically rough surface with many step bunches, that is, with a very high step density, the Stranski−Krastanov growth mechanism will lead to 3D islands or 3D crystallites. Knowing that on Ag(111), different growth temperatures, and hence different growth modes, have led to very different optical properties (i.e., different absorption or emission spectra in the visible range, fluorescence yield differing by factor 20, etc.[10]), we conclude for the present case that different preparation results of the substrate surface may lead to very different, perhaps irreproducible optical properties of the deposited organic films. We further note that seemingly identical preparation conditions may nevertheless result in different substrate surface morphologies (e.g., as a function of the cleaning cycles or as function of the substrate topography) and hence different optical and electrical properties. Thus, we conclude that the detailed control of the substrate morphology and film growth is a key for the preparation of metal−organic hybrid systems with reproducible and selected properties, at least for significantly interacting molecules such as PTCDA.

■ ASSOCIATED CONTENT

Supporting Information

The Supporting Information is available free of charge on the ACS Publications website at DOI: 10.1021/acs.langmuir.8b00493.

Movie 1 is a supplement to Figure 1 and shows the growth of PTCDA on the Au(111) surface, as observed in PEEM. The FoV is the same as in the figure. (AVI)

Movie 2 is a supplement to Figure 2and shows the desorption of PTCDA on the Au(111) surface, as observed in PEEM. The FoV is the same as in the figure. (AVI)

Movie 3 supplements Figure 5 and shows the growth of PTCDA on the Au(111) surface, as observed by LEEM, in a FoV containing both stepped and flat regions resulting in layer-by-layer and Stranki−Krastanov growth in the two regions. (AVI)

In Movie 4 (PEEM), the growth of PTCDA on Au(111) can be followed at 348 Kin a FoV of 27 μm. (AVI)

In Movie 5 (PEEM), the growth of PTCDA on Au(111) can be followed at 423 K. The movie starts with a FoV = 27 μm and continues with FoV = 55 μm. (AVI)

■ AUTHOR INFORMATION

Corresponding Author

*E-mail: schmidtt@fhi-berlin.mpg.de.

ORCID

Thomas Schmidt: 0000-0003-4389-2080

Rainer H. Fink: 0000-0002-6896-4266

Hans-Joachim Freund: 0000-0001-5188-852X

Notes

The authors declare no competing financial interest.

■ ACKNOWLEDGMENTS

Financial support by the Federal German Ministry of Education and Research (BMBF) under the contract 05 KS4WWB/4 as well as by the Max-Planck Society is gratefully acknowledged. We thank HZB for the allocation of synchrotron radiation beamtime and the BESSY-II staff, especially Matthias Mast, Fred Senf, and Christian Jung, for technical support.

DOI: 10.1021/acs.langmuir.8b00493
Langmuir 2018, 34, 5444−5453

REFERENCES

(1) Leo, K. Organic photovoltaics. *Nat. Rev. Mater.* **2016**, *1*, 16056.
(2) Hedley, G. J.; Ruseckas, A.; Samuel, I. D. W. Light Harvesting for Organic Photovoltaics. *Chem. Rev.* **2017**, *117*, 796−837.
(3) Muccini, M. A bright future for organic field-effect transistors. *Nat. Mater.* **2006**, *5*, 605−613.
(4) *Organic Light-Emitting Diodes (OLEDs), Materials, Devices and Applications*; Buckley, A., Ed.; Woodhead Publishing Limited: Oxford, Cambridge, Philadelphia, New Delhi, 2013.
(5) Choi, S.; Kwon, S.; Kim, H.; Kim, W.; Kwon, J. H.; Lim, M. S.; Lee, H. S.; Choi, K. C. Highly Flexible and Efficient Fabric-Based Organic Light-Emitting Devices for Clothing-Shaped Wearable Displays. *Sci. Rep.* **2017**, *7*, 6424.
(6) Cahen, D.; Kahn, A.; Umbach, E. Energetics of molecular interfaces. *Mater. Today* **2005**, *8*, 32−41.
(7) Otero, R.; de Parga, A. L.; Gallego, J. M. Electronic, structural and chemical effects of charge-transfer at organic/inorganic interfaces. *Surf. Sci. Rep.* **2017**, *72*, 105−145.
(8) Gebauer, W.; Langner, A.; Schneider, M.; Sokolowski, M.; Umbach, E. Luminescence quenching of ordered π-conjugated molecules near a metal surface: Quaterthiophene and PTCDA on Ag(111). *Phys. Rev. B: Condens. Matter Mater. Phys.* **2004**, *69*, 155431.
(9) Schneider, M.; Umbach, E.; Langner, A.; Sokolowski, M. Luminescence of molecules adsorbed on surfaces of wide gap materials. *J. Lumin.* **2004**, *110*, 275−283.
(10) Schneider, M.; Umbach, E.; Sokolowski, M. Growth-dependent optical properties of 3,4,9,10-perylenetetracarboxylicacid-dianhydride (PTCDA) films on Ag(111). *Chem. Phys.* **2006**, *325*, 185−192.
(11) Kilian, L.; Umbach, E.; Sokolowski, M. Molecular beam epitaxy of organic films investigated by high resolution low energy electron diffraction (SPA-LEED): 3,4,9,10-perylenetetracarboxylicacid-dianhydride (PTCDA) on Ag(111). *Surf. Sci.* **2004**, *573*, 359−378.
(12) Marchetto, H.; Schmidt, T.; Groh, U.; Maier, F. C.; Lévesque, P. L.; Fink, R. H.; Freund, H.-J.; Umbach, E. Direct observation of epitaxial organic film growth: temperature-dependent growth mechanisms and metastability. *Phys. Chem. Chem. Phys.* **2015**, *17*, 29150−29160.
(13) Marchetto, H.; Groh, U.; Schmidt, T.; Fink, R.; Freund, H.-J.; Umbach, E. Influence of substrate morphology on organic layer growth: PTCDA on Ag(111). *Chem. Phys.* **2006**, *325*, 178−184.
(14) Lévesque, P. L.; Marchetto, H.; Schmidt, T.; Maier, F. C.; Freund, H.-J.; Umbach, E. Correlation Between Substrate Morphology and the Initial Stages of Epitaxial Organic Growth: PTCDA/Ag(111). *J. Phys. Chem. C* **2016**, *120*, 19271−19279.
(15) Schmitt, S.; Schöll, A.; Umbach, E. Long-range surface faceting induced by chemisorption of PTCDA on stepped Ag(111) surfaces. *Surf. Sci.* **2016**, *643*, 59−64.
(16) Pollinger, F.; Schmitt, S.; Sander, D.; Tian, Z.; Kirschner, J.; Vrdoljak, P.; Stadler, C.; Maier, F.; Marchetto, H.; Schmidt, T.; Schöll, A.; Umbach, E. Nanoscale patterning, macroscopic reconstruction, and enhanced surface stress by organic adsorption on vicinal surfaces. *New J. Phys.* **2017**, *19*, 013019.
(17) Schmitt, S.; Schöll, A.; Umbach, E. Multitude of PTCDA Superstructures on Ag(111) and Vicinal Surfaces. *J. Phys. Chem. C* **2017**, *121*, 9860−9868.
(18) Glöckler, K.; Seidel, C.; Soukopp, A.; Sokolowski, M.; Umbach, E.; Böhringer, M.; Berndt, R.; Schneider, W.-D. Highly ordered structures and submolecular scanning tunnelling microscopy contrast of PTCDA and DM-PBDCI monolayers on Ag(111) and Ag(110). *Surf. Sci.* **1998**, *405*, 1−20.
(19) Schmitz-Hübsch, T.; Fritz, T.; Sellam, F.; Staub, R.; Leo, K. Epitaxial growth of 3,4,9,10-perylene-tetracarboxylic-dianhydride on Au(111): A STM and RHEED study. *Phys. Rev. B: Condens. Matter Mater. Phys.* **1997**, *55*, 7972−7976.
(20) Mannsfeld, S.; Toerker, M.; Schmitz-Hübsch, T.; Sellam, F.; Fritz, T.; Leo, K. Combined LEED and STM study of PTCDA growth on reconstructed Au(111) and Au(100) single crystals. *Org. Electron.* **2001**, *2*, 121−134.
(21) Nicoara, N.; Román, E.; Gómez-Rodríguez, J. M.; Martín-Gago, J. A.; Méndez, J. Scanning tunneling and photoemission spectroscopies at the PTCDA/Au(111) interface. *Org. Electron.* **2006**, *7*, 287−294.
(22) Kröger, J.; Jensen, H.; Berndt, R.; Rurali, R.; Lorente, N. Molecular orbital shift of perylenetetracarboxylic-dianhydride on gold. *Chem. Phys. Lett.* **2007**, *438*, 249−253.
(23) Kilian, L.; Umbach, E.; Sokolowski, M. A refined structural analysis of the PTCDA monolayer on the reconstructed Au(111) surface—"Rigid or distorted carpet?". *Surf. Sci.* **2006**, *600*, 2633−2643.
(24) Zou, Y.; Kilian, L.; Schöll, A.; Schmidt, T.; Fink, R.; Umbach, E. Chemical bonding of PTCDA on Ag surfaces and the formation of interface states. *Surf. Sci.* **2006**, *600*, 1240−1251.
(25) Henze, S. K. M.; Bauer, O.; Lee, T.-L.; Sokolowski, M.; Tautz, F. S. Vertical bonding distances of PTCDA on Au(111) and Ag(111): Relation to the bonding type. *Surf. Sci.* **2007**, *601*, 1566−1573.
(26) Romaner, L.; Nabok, D.; Puschnig, P.; Zojer, E.; Ambrosch-Draxl, C. Theoretical study of PTCDA adsorbed on the coinage metal surfaces, Ag(111), Au(111) and Cu(111). *New J. Phys.* **2009**, *11*, 053010.
(27) Fenter, P.; Eisenberger, P.; Burrows, P.; Forrest, S. R.; Liang, K. S. Epitaxy at the organic-inorganic interface. *Phys. B Condens. Matter* **1996**, *221*, 145−151.
(28) Forrest, S. R. Ultrathin Organic Films Grown by Organic Molecular Beam Deposition and Related Techniques. *Chem. Rev.* **1997**, *97*, 1793−1896.
(29) Capelli, R.; Mahne, N.; Koshmak, K.; Giglia, A.; Doyle, B. P.; Mukherjee, S.; Nannarone, S.; Pasquali, L. Quantitative resonant soft x-ray reflectivity of ultrathin anisotropic organic layers: Simulation and experiment of PTCDA on Au. *J. Chem. Phys.* **2016**, *145*, 024201.
(30) Fink, R.; Weiss, M. R.; Umbach, E.; Preikszas, D.; Rose, H.; Spehr, R.; Hartel, P.; Engel, W.; Degenhardt, R.; Wichtendahl, R.; Kuhlenbeck, H.; Erlebach, W.; Ihmann, K.; Schlögl, R.; Freund, H.-J.; Bradshaw, A. M.; Lilienkamp, G.; Schmidt, T.; Bauer, E.; Benner, G. SMART: A planned ultrahigh-resolution spectromicroscope for BESSY II. *J. Electron Spectrosc. Relat. Phenom.* **1997**, *84*, 231−250.
(31) Wichtendahl, R.; Fink, R.; Kuhlenbeck, H.; Preikszas, D.; Rose, H.; Spehr, R.; Hartel, P.; Engel, W.; Schlögl, R.; Freund, H.-J.; Bradshaw, A. M.; Lilienkamp, G.; Schmidt, T.; Bauer, E.; Benner, G.; Umbach, E. SMART: An aberration-corrected XPEEM/LEEM with energy filter. *Surf. Rev. Lett.* **1998**, *5*, 1249−1256.
(32) Schmidt, T.; Groh, U.; Fink, R.; Umbach, E.; Schaff, O.; Engel, W.; Richter, B.; Kuhlenbeck, H.; Schlögl, R.; Freund, H.-J. XPEEM with energy-filtering: Advantages and first results from the smart project. *Surf. Rev. Lett.* **2002**, *9*, 223−232.
(33) Rose, H.; Preikszas, D. Outline of a Versatile Corrected Leem. *Optik* **1992**, *92*, 31−44.
(34) Rose, H.; Preikszas, D. Time-Dependent Perturbation Formalism for Calculating the Aberrations of Systems with Large Ray Gradients. *Nucl. Instrum. Methods Phys. Res., Sect. A* **1995**, *363*, 301−315.
(35) Preikszas, D.; Rose, H. Correction properties of electron mirrors. *J. Electron Microsc.* **1997**, *46*, 1−9.
(36) Schmidt, T.; Marchetto, H.; Lévesque, P. L.; Groh, U.; Maier, F.; Preikszas, D.; Hartel, P.; Spehr, R.; Lilienkamp, G.; Engel, W.; Fink, R.; Bauer, E.; Rose, H.; Umbach, E.; Freund, H.-J. Double aberration correction in a low-energy electron microscope. *Ultramicroscopy* **2010**, *110*, 1358−1361.
(37) Schmidt, T.; Sala, A.; Marchetto, H.; Umbach, E.; Freund, H.-J. First experimental proof for aberration correction in XPEEM: resolution, transmission enhancement, and limitation by space charge effects. *Ultramicroscopy* **2013**, *126*, 23−32.
(38) Weiss, M. R.; Follath, R.; Sawhney, K. J. S.; Senf, F.; Bahrdt, J.; Frentrup, W.; Gaupp, A.; Sasaki, S.; Scheer, M.; Mertins, H.-C.; Abramsohn, D.; Schäfers, F.; Kuch, W.; Mahler, W. The elliptically polarized undulator beamlines at BESSY II. *Nucl. Instrum. Methods Phys. Res., Sect. A* **2001**, *467*, 449−452.
(39) Bauer, E. Low energy electron microscopy. *Rep. Prog. Phys.* **1994**, *57*, 895−938.

DOI: 10.1021/acs.langmuir.8b00493
Langmuir 2018, 34, 5444−5453

(40) Zhou, Y.; Fuentes-Hernandez, C.; Shim, J.; Meyer, J.; Giordano, A. J.; Li, H.; Winget, P.; Papadopoulos, T.; Cheun, H.; Kim, J.; Fenoll, M.; Dindar, A.; Haske, W.; Najafabadi, E.; Khan, T. M.; Sojoudi, H.; Barlow, S.; Graham, S.; Bredas, J.-L.; Marder, S. R.; Kahn, A.; Kippelen, B. A universal method to produce low-work function electrodes for organic electronics. *Science* **2012**, *336*, 327−332.
(41) Bagus, P. S.; Staemmler, V.; Wöll, C. Exchangelike effects for closed-shell adsorbates: interface dipole and work function. *Phys. Rev. Lett.* **2002**, *89*, 096104.
(42) Bagus, P. S.; Hermann, K.; Wöll, C. The interaction of C6H6 and C6H12 with noble metal surfaces: electronic level alignment and the origin of the interface dipole. *J. Chem. Phys.* **2005**, *123*, 184109.
(43) Tautz, F. S. Structure and bonding of large aromatic molecules on noble metal surfaces: The example of PTCDA. *Prog. Surf. Sci.* **2007**, *82*, 479−520.
(44) Tautz, F. S.; Eremtchenko, M.; Schaefer, J. A.; Sokolowski, M.; Shklover, V.; Glöckler, K.; Umbach, E. A comparison of the chemisorption behaviour of PTCDA on different Ag surfaces. *Surf. Sci.* **2002**, *502*, 176−184.
(45) Taborski, J.; Väterlein, P.; Dietz, H.; Zimmermann, U.; Umbach, E. NEXAFS investigations on ordered adsorbate layers of large aromatic molecules. *J. Electron Spectrosc. Relat. Phenom.* **1995**, *75*, 129−147.
(46) Shklover, V.; Tautz, F. S.; Scholz, R.; Sloboshanin, S.; Sokolowski, M.; Schaefer, J. A.; Umbach, E. Differences in vibronic and electronic excitations of PTCDA on Ag(111) and Ag(110). *Surf. Sci.* **2000**, *454*, 60−66.
(47) Wießner, M.; Hauschild, D.; Sauer, C.; Feyer, V.; Schöll, A.; Reinert, F.; Reinert, F. Complete determination of molecular orbitals by measurement of phase symmetry and electron density. *Nat. Commun.* **2014**, *5*, 4156.
(48) Lovinger, A. J.; Forrest, S. R.; Kaplan, M. L.; Schmidt, P. H.; Venkatesan, T. Structural and Morphological Investigation of the Development of Electrical-Conductivity in Ion-Irradiated Thin-Films of an Organic Material. *J. Appl. Phys.* **1984**, *55*, 476−482.
(49) Möbus, M.; Karl, N.; Kobayashi, T. Structure of Perylene-Tetracarboxylic-Dianhydride Thin-Films on Alkali-Halide Crystal Substrates. *J. Cryst. Growth* **1992**, *116*, 495−504.
(50) Iqbal, Z.; Ivory, D. M.; Eckhardt, H. Synthesis, Crystal-Structure and Spectroscopy of 3,4-Perylenedicarboxylic Monoanhydride. *Mol. Cryst. Liq. Cryst.* **1988**, *158*, 337−352.
(51) Stöhr, J. *NEXAFS Spectroscopy*; Springer: Berlin, Heidelberg, 1992.
(52) Schöll, A.; Zou, Y.; Schmidt, T.; Fink, R.; Umbach, E. Energy calibration and intensity normalization in high-resolution NEXAFS spectroscopy. *J. Electron Spectrosc. Relat. Phenom.* **2003**, *129*, 1−8.
(53) Bowker, M. The Role of Precursor States in Adsorption, Surface Reactions and Catalysis. *Top. Catal.* **2016**, *59*, 663−670.
(54) Hauschild, A.; Karki, K.; Cowie, B. C. C.; Rohlfing, M.; Tautz, F. S.; Sokolowski, M. Molecular distortions and chemical bonding of a large pi-conjugated molecule on a metal surface. *Phys. Rev. Lett.* **2005**, *94*, 036106.
(55) Kilian, L.; Hauschild, A.; Temirov, R.; Soubatch, S.; Schöll, A.; Bendounan, A.; Reinert, F.; Lee, T.-L.; Tautz, F. S.; Sokolowski, M.; Umbach, E. Role of intermolecular interactions on the electronic and geometric structure of a large pi-conjugated molecule adsorbed on a metal surface. *Phys. Rev. Lett.* **2008**, *100*, 136103.

DOI: 10.1021/acs.langmuir.8b00493
Langmuir 2018, 34, 5444−5453